APL Materials

High-k perovskite gate oxide $BaHfO_3$

Cite as: APL Mater. **5**, 016104 (2017); https://doi.org/10.1063/1.4974864
Submitted: 21 November 2016 • Accepted: 04 January 2017 • Published Online: 26 January 2017

Young Mo Kim, Chulkwon Park, Taewoo Ha, et al.

APL MATERIALS **5**, 016104 (2017)

High-k perovskite gate oxide $BaHfO_3$

Young Mo Kim,[1] Chulkwon Park,[1,a] Taewoo Ha,[2] Useong Kim,[1,a] Namwook Kim,[3] Juyeon Shin,[1] Youjung Kim,[1] Jaejun Yu,[3] Jae Hoon Kim,[2] and Kookrin Char[1,b]

[1]*Department of Physics and Astronomy, Institute of Applied Physics, Seoul National University, Seoul 08826, South Korea*
[2]*Department of Physics, Yonsei University, Seoul 03722, South Korea*
[3]*Center for Theoretical Physics, Department of Physics and Astronomy, Seoul National University, Seoul 08826, South Korea*

(Received 21 November 2016; accepted 4 January 2017; published online 26 January 2017)

We have investigated epitaxial $BaHfO_3$ as a high-k perovskite dielectric. From x-ray diffraction measurement, we confirmed the epitaxial growth of $BaHfO_3$ on $BaSnO_3$ and MgO. We measured optical and dielectric properties of the $BaHfO_3$ gate insulator; the optical bandgap, the dielectric constant, and the breakdown field. Furthermore, we fabricated a perovskite heterostructure field effect transistor using epitaxial $BaHfO_3$ as a gate insulator and La-doped $BaSnO_3$ as a channel layer on $SrTiO_3$ substrate. To reduce the threading dislocations and enhance the electrical properties of the channel, an undoped $BaSnO_3$ buffer layer was grown on $SrTiO_3$ substrates before the channel layer deposition. The device exhibited a field effect mobility value of 52.7 cm^2 V^{-1} s^{-1}, a I_{on}/I_{off} ratio higher than 10^7, and a subthreshold swing value of 0.80 V dec^{-1}. We compare the device performances with those of other field effect transistors based on $BaSnO_3$ channels and different gate oxides. [http://dx.doi.org/10.1063/1.4974864]

High-*k* dielectric materials have been extensively investigated during the last decade to overcome the gate leakage problem of SiO_2.[1] The SiO_2 layer thickness required for gate dielectrics nowadays is so thin (~1 nm) that the leakage current would exceed 1 A cm^{-2}, causing unacceptably high power dissipation. High-*k* dielectrics were introduced to solve this issue and binary oxides such as HfO_2, Al_2O_3, and ZrO_2 were investigated.[2–4] In early 2000s, HfO_2 was primarily studied and transistors with Hf-based high-*k* dielectrics were already commercially manufactured.[1,5] HfO_2 displays good thermal stability with the Si substrate and can be deposited by atomic layer deposition which produces an atomically smooth layer.[1,6] However, HfO_2 still needs to be improved in terms of its interfacial quality and low crystallization temperature. Other high-*k* dielectrics have also been investigated for future high-*k* dielectrics not only to replace SiO_2 but also to be used with other semiconductors such as Ge or GaN, in cases where Si loses the advantage of its high quality Si/SiO_2 interface. In the case of Ge, for example, high-*k* materials such as HfO_2, La_2O_3, $BaTiO_3$, and $SrHfO_3$ have been studied.[7–9] AlGaN is mostly used with GaN to construct high electron mobility transistors, and high-*k* dielectrics on top of AlGaN have been tried to achieve normally off operation.[10,11] Among various high-*k* materials, perovskite oxides such as $SrTiO_3$ and $BaTiO_3$ have been investigated as a gate oxide due to their high dielectric constant as well as their functional properties such as superconductivity, ferroelectricity, and ferromagnetism.[1,12–16] However, the stability of such titanates is expected to become an issue.

Recent discovery of high mobility larger than 300 cm^2 V^{-1} s^{-1} at room temperature and stability in the perovskite stannate[17] has created a need to find compatible perovskite high-*k* dielectric materials.

[a]Currently at Samsung Electronics, Suwon, South Korea.
[b]Author to whom correspondence should be addressed. Electronic mail: kchar@phya.snu.ac.kr

$LaInO_3$ was identified as one of such epitaxial polar perovskite dielectrics and successfully used as a gate oxide on the top of $BaSnO_3$.[18] Subsequently, the interfaces between $LaInO_3$ and $BaSnO_3$ were reported to display a large conductance enhancement due to the polar nature of $LaInO_3$.[19] Another epitaxial perovskite high-k dielectric material, especially of a non-polar structure, will be of large interest for its own use as a high-*k* gate oxide but for comparison of its interface properties with $BaSnO_3$ as well.

$BaHfO_3$ (BHO) is such a nonpolar cubic perovskite oxide with a high dielectric constant and a large bandgap. BHO, Hf-based alkaline earth perovskites, was investigated by some groups for application as a dielectric,[20,21] especially as a next generation alternative for HfO_2. There exist a few reports regarding dielectric properties of BHO films that measured their dielectric constants as 23–45.[20–23] However, to our knowledge, no field effect transistor (FET) using BHO as a gate insulator has been fabricated. Perovskite structure of BHO, in addition to the high dielectric constant, is also advantageous, for various physical properties of other perovskite oxides which can be incorporated into a common crystal structure. In this paper, we describe the carrier modulation of the La-doped $BaSnO_3$ (BLSO) channel, a perovskite semiconductor with high electron mobility, via field effect through BHO.

All samples were grown by pulsed-laser deposition at 750 °C with an oxygen pressure of 100 mTorr. We used a KrF excimer laser with 248 nm wavelength at the energy fluence about 1–1.5 J cm^{-2}. All targets were provided by Toshima Manufacturing, Co., in Japan. Stencil masks made of Si or stainless steel were used to make lateral patterns of samples. Electrical measurements were performed using the Keithley 4200 semiconductor characterization system.

We first investigated the epitaxial growth of the BHO layer on $BaSnO_3$ (BSO) layer by x-ray diffraction measurement. The measured sample was 100 nm thick BHO layer deposited on the top of a 10 nm thick BSO film on a $SrTiO_3$ substrate. BSO layer thickness was minimized to reduce possible peaks from BSO. $\theta - 2\theta$ diffraction pattern in Figure 1(a) shows peaks corresponding to the (001) direction without any peaks from other directions, indicating that BHO is epitaxially grown on BSO at the (001) direction. Small full width at half maximum presented in the inset also verifies high crystallinity of BHO on BSO. To obtain the lattice parameters of BHO, reciprocal space mapping (RSM) was performed on the BHO (103) peak. From the measured reciprocal space vectors Q_x = 1.516 Å^{-1} and Q_z = 4.506 Å^{-1} shown in Figure 1(b), we obtained in-plane lattice parameters a = 4.145 Å and c = 4.183 Å. Compared with the lattice parameters of bulk BHO a = 4.171 Å, this result indicates that BHO is compressively strained due to BSO which has the lattice constant 4.116 Å.[17,24]

Figure 2(a) shows the optical absorption measurement of the BHO film to determine the optical band gap (E_g). We used an r-Al_2O_3 (E_g ~ 9 eV) substrate to avoid absorption from the substrate. Thin MgO (E_g ~ 8 eV) layer was deposited as a buffer layer, which is known to epitaxially grow

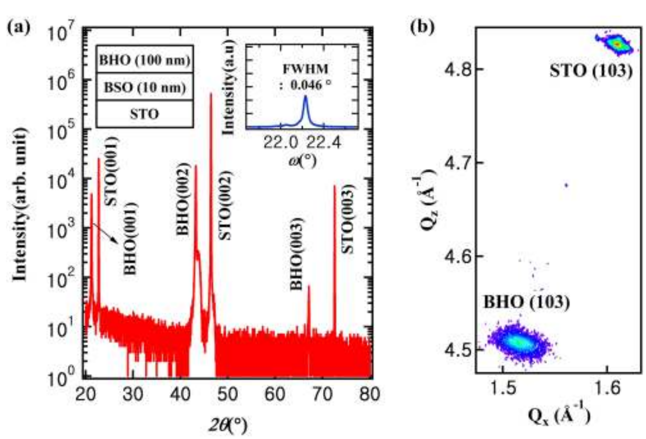

FIG. 1. X-ray diffraction pattern of the BHO thin film. (a) $\theta - 2\theta$ diffraction pattern shows diffraction peaks corresponding to (001), (002), and (003) of BHO. Small peak around (002) of BHO is (002) peak of BSO. ω-rocking curve presented as an inset was measured at the (002) peak of BHO. (b) The reciprocal space map of (103) plane of BHO.

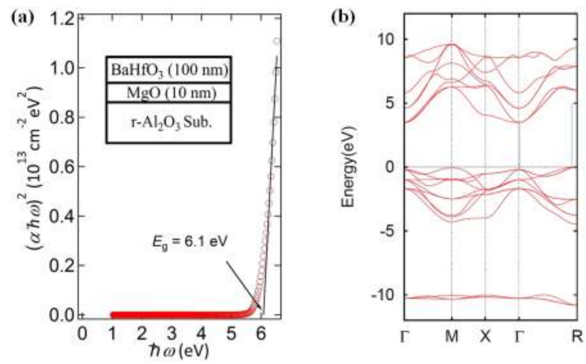

FIG. 2. Optical absorption and electronic band structure of BHO. (a) The absorbance of the BHO/MgO/r-sapphire substrate was measured. Assuming zero reflectance, $(\alpha\hbar\omega)^2$ vs. $\hbar\omega$ plot is constructed. The black line is the line of extrapolation which shows that the BHO film has a direct band gap with a magnitude of about 6.1 eV. (b) We performed the first-principle calculations and obtained the electronic band structure of BHO.

on r-Al_2O_3.[25] The optical absorption coefficient (α) was evaluated from the formula in the case of negligible reflectance,[26]

$$\alpha = \frac{1}{d}\ln\frac{1}{T},$$

where d and T are the thickness and the transmittance of the film, respectively. The band gap of BHO was evaluated by Tauc's plot method,

$$(\alpha\hbar\omega)^{\mathrm{n}} = A(\hbar\omega - E_g),$$

where $\hbar\omega$, A, and E_{g} are the light energy, a constant, and the optical band gap, respectively. The Tauc plot for n = 2 shows a distinct linear region, implying direct optical transition. The optical band gap of BHO was evaluated to be 6.1 eV by a linear extrapolation of the graph. Figure 2(b) is the band structure of BHO obtained from the first-principle calculation. The direct band gap at Γ point is 3.6 eV, which is 40% smaller than the measured optical band gap, but underestimation of the band gap often occurs in the local density approximation.[27] We estimated electron effective mass at conduction band minimum of BHO to be $0.62m_0$, which will be used later in the paper for Fowler-Nordheim (FN) analysis.

In order to measure the dielectric properties of BHO, we fabricated a capacitor made of a 97 nm thick BHO layer inserted between 4% BLSO electrodes with an area of 8000 μm^2. AC voltage with 30 mV root-mean square amplitude was applied to obtain admittance from which the parallel capacitance (C_{p}) and dissipation factor (tan δ) were evaluated. Figure 3(a) shows the measured C_{p} and tan δ at various frequencies. From the measured C_{p}, the dielectric constant (κ) of BHO is calculated to be 37.8, which is consistent with the value reported in previous publications.[20–23] We also measured C_{p} while varying the DC bias and found that C_{p} was nearly constant with less than 2% variation from its average value as shown in Figure S1 of the supplementary material, which implies BHO is a linear dielectric material. The breakdown field (E_{BD}) was evaluated by measuring the leakage current through the capacitor. As shown in Figure 3(b), E_{BD} occurred at 3.6 MV/cm. From the measured κ and E_{BD}, we obtained the maximum field-induced charge density of BHO to be as high as 7.5×10^{13} cm^{-2}.

The leakage current before dielectric breakdown can be used to calculate the barrier height between BLSO and BHO. Fowler-Nordheim (FN) tunneling through an insulator in a high electric field is described by the relation

$$J \propto E^2 \exp\left(\frac{-4\sqrt{2m^*_{diel}}\Phi^{3/2}}{3e\hbar E}\right),$$

where J, m^*_{diel}, E, and Φ are the current density, the electric field, the effective mass of conduction electrons in the insulator, and the barrier height, respectively. We plotted $\ln(J/E^2)$ versus E^{-1} in the

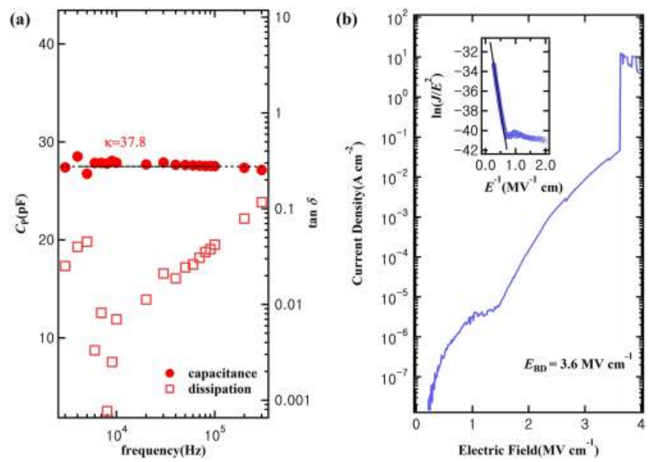

FIG. 3. Dielectric properties of BHO. (a) The capacitance of the BHO dielectric layer inserted between 4% BLSO contacts was measured with respect to the applied frequencies of AC voltage. κ was calculated from the measured capacitance and the dimensions of the capacitor. (b) J-E characteristic of the BHO capacitor. The inset graph of ln(J/E^2) vs. E^{-1} is plotted to confirm the FN tunneling process in the BHO layer. The black line is the linear fit from which we calculated the barrier height at the BHO/BLSO interface.

inset of Figure 3(b) to check whether the FN analysis is appropriate for the conduction mechanism of BHO. We confirmed that the data were well fitted with a line in the high electric field region, which indicates that the FN tunneling is the dominant mechanism of the leakage current in the high electric field. Using the slope of the line and effective mass of BHO obtained in the band structure calculation, we estimated $\Phi = 0.51$ eV. To calculate the conduction band offset, we need to know the energy level difference between the conduction band and fermi level of 4% BLSO. Assuming a parabolic band, carrier concentration and fermi level have the following relation in the degenerate doping region:

$$n = N_C \frac{4\eta_c^{3/2}}{3\sqrt{\pi}}, \quad \eta_c = \frac{E_F - E_C}{k_B T}, \quad N_C = 2\left[\frac{m_n^* k_B T}{2\pi\hbar^2}\right]^{3/2},$$

where n, m_n^*, E_F, E_C, and T are the carrier concentration, the effective mass of the conduction electrons, the Fermi level, the energy level of the conduction band minimum, and the temperature, respectively. Using $m_n^* = 0.42m_0$, $n = 5.0 \times 10^{20}$ cm^{-3} for 4% BLSO, we calculated $E_F - E_C$ to be 0.55 eV. The conduction band offset is found to be 1.06 eV, which is the sum of Φ and $E_F - E_C$, smaller value than the previously reported value of 1.9 eV.[21,28] Since the FN analysis assumes, for perfect bulk dielectrics with no defects, the leakage current is dominant by tunneling through partial width of the barrier, underestimation of barrier height is not surprising for a realistic dielectric material with some defects.

Employing BHO as a gate oxide and BLSO as a channel, we fabricated a field effect device. Figure 4(a) shows a cross-sectional diagram of the device. We first deposited a 150 nm BSO buffer layer to reduce the effect of threading dislocations on electrical properties of the BLSO channel layer.[29] The deposition of a 12-nm-thick 0.5% BLSO channel layer using a Si mask was followed. After the growth of 4% BLSO contact layer through a stainless steel mask, a 126 nm-thick BHO dielectric layer was grown using another Si mask. As the final step, 4% BLSO contact was grown on the top of the BHO dielectric layer as a gate electrode using a Si mask. Figure 4(b) is the microscope image of the actual device.

The output characteristics of the device are presented in Figure 4(c). The source-drain voltage (V_{DS}) was applied up to 10 V while the gate voltage (V_{GS}) varied from 8 to −1 V with the interval of 1 V. The device exhibited a clear n-type FET behavior. We could observe that the source-drain current (I_{DS}) is proportional to V_{DS} at low V_{DS} and deviates from linear behavior as V_{DS} increases. As V_{GS} changes from 8 to −1 V, I_{DS} also decreases along with V_{GS}, which is consistent with the behavior of a standard n-type FET.

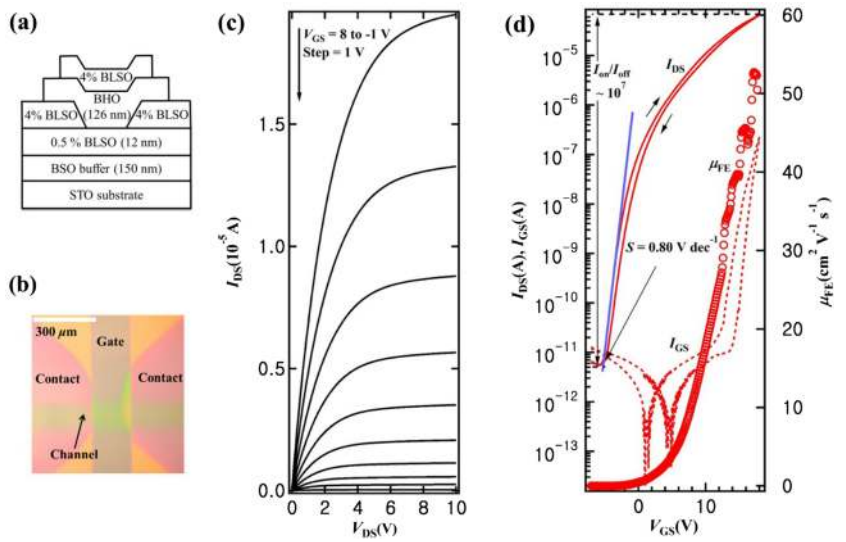

FIG. 4. Structure and I-V characteristics of the BHO/BLSO field effect transistor. (a) Cross-sectional diagram of the device. (b) The top view of the device pictured by an optical microscope. (c) The output characteristic of the device. V_{GS} was varied from 8 V to −1 V with 1 V interval. (d) Transfer characteristics of the device at V_{DS} = 1 V. The maximum value of μ_{FE} is 52.7 cm^2/Vs. I_{on}/I_{off} and S are 10^7 and 0.80 V/dec, respectively.

The transfer characteristics are shown in Figure 4(d). I_{DS} and gate leakage current (I_{GS}) were measured at V_{DS} = 1 V while V_{GS} was swept from −7 V to 18 V. We confirmed sufficient current enhancement in applying a positive V_{GS}. Several important static characteristics of FET were extracted from the transfer characteristics. I_{on}/I_{off} ratio, defined as the ratio of the maximum to minimum I_{DS}, is about 10^7. The subthreshold swing S was evaluated from the relation $S = [\partial \log_{10}(I_{DS})/\partial V_{GS}]^{-1}$ as 0.80 V dec^{-1}. The field effect mobility (μ_{FE}) was calculated using the relation

$$\mu_{FE} = \left(\frac{Lt}{W\kappa\varepsilon_0 V_{DS}}\right)\frac{\partial I_{DS}}{\partial V_{GS}},$$

where L, t, W, and ϵ_0 are the channel length, the thickness of the BHO layer, the channel width, and the permittivity of the vacuum, respectively. The maximum μ_{FE} was evaluated to be 52.7 cm^2 V^{-1} s^{-1}. We also measured the capacitance between the gate and the source while varying V_{GS} and evaluated the AC conductance to further estimate dielectric and interfacial properties of the device, as described in Figures S2 and S3 of the supplementary material.

Compared with other FETs based on BLSO channels, our FET exhibited better μ_{FE} and I_{on}/I_{off} ratio than those with amorphous gate oxides HfO_2 or Al_2O_3.[29,30] This enhanced performance can be attributed to reduced interfacial charge traps due to the epitaxial perovskite structure of BHO and BLSO. On the other hand, compared with the other FET which used the perovskite $LaInO_3$ (LIO) dielectric layer and BLSO channels, our FET showed smaller μ_{FE} and similar I_{on}/I_{off} ratio.[18] Since the doping level of the BLSO channel in our case is 0.5% while that of LIO/BLSO FET is 0.07%, the increased impurity scattering is probably responsible for the reduced μ_{FE}. Recently reported FETs successfully used a 10 nm thick epitaxial perovskite $Sr_{0.5}Ba_{0.5}SnO_3$ (SBSO) dielectric layer in combination with organic polymer parylene as the gate oxide on the undoped BSO channel.[31] Our BHO/BLSO interface and SBSO/BSO interface showed similar μ_{FE} despite the existence of impurity scattering in the BLSO channel. In the case of the BHO/BLSO interface, V_{GS} needed to modulate the channel conductance is lower by one order of magnitude compared with that of the SBSO/BSO interface, consistent with the high dielectric constant of BHO.

In summary, we investigated the dielectric properties of BHO and applied BHO to a FET with the BLSO channel. We confirmed the epitaxial growth of BHO on BSO and characterized the dielectric properties, optical bandgap, and the conduction band offset with BSO. In FETs, we achieved μ_{FE} of 52.7 cm^2 V^{-1} s^{-1} and I_{on}/I_{off} higher than 10^7, which are better than those of other FETs with amorphous gate oxides based on the BLSO channel. We believe that the improved device performance can be attributed to the epitaxial perovskite structure of BHO. Use of multiple layers of dielectrics tailored with the appropriate channel doping will lead to further enhancement of the device performances.

See supplementary material for the field-dependence of the BHO dielectric properties, the capacitance-gate voltage measurement, and the AC conductance measurement of the FET device.

This work is partially supported by Samsung Science and Technology Foundation under Project No. SSTF-BA1402-09.

[1] J. Robertson and R. M. Wallace, Mater. Sci. Eng., R **88**, 1 (2015).
[2] G. D. Wilk, R. M. Wallace, and J. M. Anthony, J. Appl. Phys. **89**, 10 (2001).
[3] D. G. Park, H. J. Cho, K. Y. Lim, C. Lim, I. S. Yeo, J. S. Roh, and J. W. Park, J. Appl. Phys. **89**(11), 6275 (2001).
[4] R. Puthenkovilakam and J. P. Chang, J. Appl. Phys. **96**, 5 (2004).
[5] K. Mistry, C. Allen, C. Auth, B. Beattie, D. Bergstrom, M. Bost, M. Brazier, M. Buehler, A. Cappellani, R. Chau, C. H. Choi, G. Ding, K. Fischer, T. Ghani, R. Grover, W. Han, D. Hanken, M. Hattendorf, J. He, J. Hicks, R. Huessner, D. Ingerly, P. Jain, R. James, L. Jong, S. Joshi, C. Kenyon, K. Kuhn, K. Lee, H. Liu, J. Maiz, B. McIntyre, P. Moon, J. Neirynck, S. Pae, C. Parker, D. Parsons, C. Prasad, L. Pipes, M. Prince, P. Ranade, T. Reynolds, J. Sandford, L. Shifren, J. Sebastian, J. Seiple, D. Simon, S. Sivakumar, P. Smith, C. Thomas, T. Troeger, P. Vandervoorn, S. Williams, and K. Zawadzki, in *2007 IEEE International Electron Devices Meeting* (IEEE, 2007), p. 247.
[6] J. H. Choi, Y. Mao, and J. P. Chang, Mater. Sci. Eng., R **72**, 97 (2011).
[7] K. Kita, T. Takahashi, H. Nomura, S. Suzuki, T. Nishimura, and A. Toriumi, Appl. Surf. Sci. **254**, 6100 (2008).
[8] K. D. Fredrickson, P. Ponath, A. B. Posadas, M. R. McCartney, T. Aoki, D. J. Smith, and A. A. Demkov, Appl. Phys. Lett. **104**, 242908 (2014).
[9] M. D. McDaniel, C. Hu, S. Lu, T. Q. Ngo, A. Posadas, A. Jiang, D. J. Smith, E. T. Yu, A. A. Demkov, and J. G. Ekerdt, J. Appl. Phys. **117**, 054101 (2015).
[10] T. Imada, M. Kanamura, and T. Kikkawa, in *Power Electronics Conference (IPEC)* (IEEE, 2010), p. 1027.
[11] T. E. Hsieh, E. Y. Chang, Y. Z. Song, Y. C. Lin, H. C. Wang, S. C. Liu, S. Salahuddin, and C. C. Hu, IEEE Electron Device Lett. **35**, 732 (2014).
[12] R. A. McKee, F. J. Walker, and M. F. Chisholm, Phys. Rev. Lett. **81**, 3014 (1998).
[13] R. Droopad, Z. Yu, J. Ramdani, L. Hilt, J. Curless, C. Overgaard, J. L. Edwards, Jr., J. Finder, K. Eisenbeiser, and W. Ooms, Mater. Sci. Eng., B **87**, 292 (2001).
[14] A. A. Demkov, A. B. Posadas, H. Seo, M. Choi, K. J. Kormondy, P. Ponath, R. C. Hatch, M. D. McDaniel, T. Q. Ngo, and J. G. Ekerdt, ECS Trans. **54**, 255 (2013).
[15] M. Ben Shalom, M. Sachs, D. Rakhmilevitch, A. Palevski, and Y. Dagan, Phys. Rev. Lett. **104**, 1 (2010).
[16] M. B. Smith, K. Page, T. Siegrist, P. L. Redmond, E. C. Walter, R. Seshadri *et al.*, J. Am. Chem. Soc. **130**, 6955 (2008).
[17] H. J. Kim, U. Kim, H. M. Kim, T. H. Kim, H. S. Mun, B. G. Jeon, K. T. Hong, W. J. Lee, C. Ju, K. H. Kim, and K. Char, Appl. Phys. Express **5**, 061102 (2012).
[18] U. Kim, C. Park, T. Ha, Y. M. Kim, N. Kim, C. Ju, J. Park, J. Yu, J. H. Kim, and K. Char, APL Mater. **3**, 036101 (2015).
[19] U. Kim, C. Park, Y. M. Kim, J. Shin, and K. Char, APL Mater. **4**, 071102 (2016).
[20] G. Lupina, G. Kozlowski, P. Dudek, J. Dabrowski, Ch. Wenger, G. Lippert, and H. J. Müssig, in *2008 9th International Conference on Ultimate Integration of Silicon (ULIS)* (IEEE, 2008), p. 159.
[21] G. Lupina, O. Seifarth, P. Dudek, G. Kozlowski, J. Dabrowski, H. J. Thieme, G. Lippert, T. Schroeder, and H. J. Müssig, Phys. Status Solidi B **248**, 323 (2011).
[22] A. Feteira, D. C. Sinclair, K. Z. Rajab, and M. T. Lanagan, J. Am. Ceram. Soc. **91**, 893 (2008).
[23] G. Lupina, G. Kozłowski, J. Dabrowski, Ch. Wenger, P. Dudek, P. Zaumseil, G. Lippert, Ch. Walczyk, and H. J. Müssig, Appl. Phys. Lett. **92**, 062906 (2008).
[24] T. Maekawa, K. Kurosaki, and S. Yamanaka, J. Alloys Compd. **407**, 44 (2006).
[25] K. Char, M. S. Colclough, S. M. Garrison, N. Newman, and G. Zaharchuk, Appl. Phys. Lett. **59**, 733 (1991).
[26] V. Kumar, R. G. Singh, L. P. Purohit, and R. M. Mehra, J. Mater. Sci. Technol. **27**, 481 (2011).
[27] M. Hussein, N. Assadi, and D. A. H. Hanaor, J. Appl. Phys. **113**, 233913 (2013).
[28] U. Kim, Ph.D. thesis, Seoul National University, 2015.
[29] C. Park, U. Kim, C. J. Ju, J. S. Park, Y. M. Kim, and K. Char, Appl. Phys. Lett. **105**, 203503 (2014).
[30] Y. M. Kim, C. Park, U. Kim, C. Ju, and K. Char, Appl. Phys. Express **9**, 011201 (2016).
[31] K. Fujiwara, K. Nishihara, J. Shiogai, and A. Tsukazaki, AIP Adv. **6**, 085014 (2016).